

HiSST: 4th International Conference on High-Speed Vehicle Science Technology 22 -26 September 2025, Tours, France



Mid-Course Trajectory Optimization for Variable Flow Ducted Rocket Missile under Radar Detection Angle Constraint

Heun-Jae Lee¹, Boseok Kim¹, Chang-Hun Lee¹, Min-Jea Tahk¹, Chul Lee², Byung-Gi Kwon², Koang-Kyu Jeon²

Abstract

A variable flow ducted rocket (VFDR) engine offers a broader operational envelope than ramjet engines, as well as higher energy efficiency and a more flexible thrust modulation capability than conventional solid-fuel rocket engines, making it well-suited for long-range air-to-air missile applications. For such missiles, appropriate mid-course guidance toward the predicted intercept point (PIP) is essential prior to seeker's lock-on. However, due to the high maneuverability of aerial targets, the PIP may vary significantly over time, necessitating adaptive mid-course guidance strategies. As a preliminary investigation into this challenge, this study performs trajectory optimization for a VFDR missile considering radar field-of-view (FOV) constraints for data link communication between the fighter and the missile. The results indicate that radar FOV constraints can affect the optimal trajectory, particularly when the target is relatively close and at higher altitudes.

Keywords: Variable Flow Ducted Rocket Missile, Trajectory Optimization, Radar Detection Angle Constraint, Pseudo-spectral Convex Programming

Nomenclature

AF – Air to Fuel ratio

 $C_{L_{\alpha}}$ – Lift coefficient

 C_{D_0} – Drag coefficient

D — Drag force

 F_i – Equations of motion for each state

g – Gravitational constant

G − Air mass flow rate function

h – Altitude

i, j, k, n – Positive integer index

 l_u , l_d – Upward & Downward radar FOV limits

m – Mass

 P_n – nth order Legendre polynomial

T — Thrust

u, U – Control inputs

V - Velocity

x – Downrange

Z - State vector

 α – Angle of attack

 γ – Flight path angle

ζ – Step size in line search

 η – Total flight time

 μ_1 , μ_2 – Penalty weights in the merit function

 τ – Normalized time

¹ Department of Aerospace Engineering, KAIST, Daejeon, Korea, gmswo0217@kaist.ac.kr

¹ Department of Aerospace Engineering, KAIST, Daejeon, Korea, kbobo6@kaist.ac.kr

¹ Department of Aerospace Engineering, KAIST, Daejeon, Korea, lckdgns@kaist.ac.kr

¹ Department of Aerospace Engineering, KAIST, Daejeon, Korea, mjtahk317@qmail.com

² LIG Nex1, Daejeon, Korea, leechul@lignex1.com

² LIG Nex1, Daejeon, Korea, byunggi.kwon2@lignex1.com

² LIG Nex1, Daejeon, Korea, koangkyu.jeon@lignex1.com



HiSST: 4th International Conference on High-Speed Vehicle Science Technology

22 -26 September 2025, Tours, France



1. Introduction

A variable flow ducted rocket (VFDR) engine is a propulsion system that combines the advantages of solid-fuel rockets and ramjet engines. Like a ramjet, the VFDR intakes ambient air and uses it as an oxidizer, which allows it to carry more fuel on board and thereby extend the flight range. However, there exist slight differences. Unlike a ramjet engine, the VFDR carries some amount of onboard oxidizer. This oxidizer is combined with fuel in a gas generator to produce partially combusted gas. The resulting gas is then mixed with compressed air and burned in the ram combustor to generate thrust. This two-stage combustion mechanism improves combustion stability, ensuring high maneuverability without flameout. Additionally, the VFDR engine has a valve between the gas generator and the ram combustor which regulates the fuel mass flow rate. This allows the missile to utilize its fuel in the latter part of the flight, thereby achieving high terminal velocity. Given these advantages, the VFDR engine is widely recognized as a suitable propulsion system for long-range air-to-air missiles, exemplified by the Meteor missile.

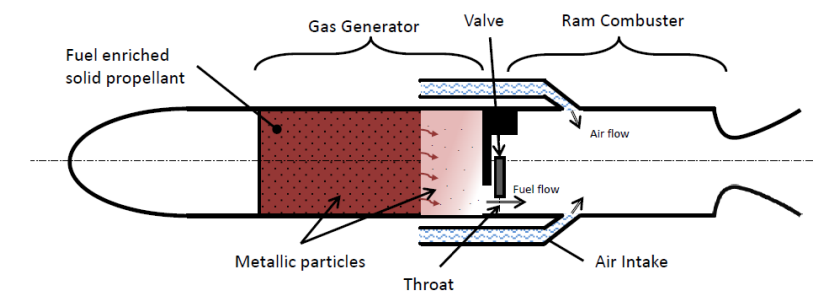


Fig 1. VFDR Configuration [1]

Meanwhile, long-range air-to-air missiles are often referred to as beyond-visual-range air-to-air missiles (BVRAAMs), as they are launched before the seeker acquires the target. In such cases, mid-course guidance is employed, and the missile is guided toward the predicted intercept point (PIP) to achieve seeker's lock-on. Given that VFDR-based missiles, such as the Meteor, have a maximum range of approximately 200–300km, the majority of the flight occurs in the mid-course phase before terminal guidance is initiated, which typically takes place within about 30km of the target. Consequently, guidance strategy during mid-course phase might be critical to overall interception performance.

In air-to-air engagements, the target—typically an enemy fighter aircraft—possesses high speed and agility, enabling rapid evasive maneuvers. When a missile is launched from several hundred kilometers away, such maneuvers can significantly alter the predicted intercept point (PIP). To cope with changes in the PIP, the optimal trajectory has to be updated periodically updated. This, in turn, necessitates a data link between the missile and the launching fighter aircraft, which provides up-to-date target information until the seeker achieves lock-on in the terminal phase. Consequently, both the target and the missile must remain within the radar's detection angle. In this study, it is assumed that the data link is established via the radar of the fighter aircraft, and the missile's midcourse trajectory is planned so as to meet the radar's detection constraints. This trajectory planning problem is accordingly formulated as an optimal control problem and solved.

The solution methods for optimal control problems can be broadly categorized into two primary approaches: indirect methods and direct methods. Indirect methods solve the problem by deriving the necessary conditions for optimality—such as those given by Pontryagin's Maximum Principle—and can, in some cases, yield analytical solutions. However, deriving such solutions can be mathematically challenging, and these methods often face limitations in handling multiple constraints simultaneously. To address these drawbacks, approximation techniques such as singular perturbation methods have been proposed to reduce the order of the problem [2], [3]. Nevertheless, these approaches typically rely on strong assumptions, such as time-scale separation, and the resulting guidance may violate constraints.

On the other hand, direct methods discretize the continuous-time optimal control problem into a finite-dimensional optimization problem, which can be solved using various nonlinear programming (NLP) algorithms without explicitly deriving the necessary conditions for optimality. In recent years, sequential convex programming (SCP) has attracted attention as an efficient approach for such problems. Although SCP does not offer formal guarantees of convergence or global optimality, it offers computational efficiency and has been successfully applied in aerospace applications [4–7]. In particular, the PSCP method proposed in [5] employs pseudospectral techniques to discretize the system dynamics, thereby achieving high accuracy with relatively few nodes. In addition, [6] and [7] incorporated a line search procedure into the SCP framework to improve convergence.

Motivated by these studies, the present work adopts the PSCP framework to accurately approximate the long-range flight trajectory of the VFDR missile and incorporates a line search algorithm to enhance convergence. Furthermore, as discussed in Section 3.3, some modifications to the existing Improved Trust Region Method are introduced in an effort to enhance its convergence characteristics for VFDR missile trajectory optimization problem.

The rest of the paper is organized as follows. Section 2 formulates the optimal control problem for the mid-course guidance of a VFDR missile. Section 3 presents the procedure for obtaining the optimal solution using the pseudospectral sequential convex programming (PSCP) method combined with the proposed method. Finally, Section 4 evaluates the necessity of the radar field-of-view constraint and assesses the performance and validity of the proposed method.

2. Problem Formulation

In this section, the optimal control problem for mid-course trajectory optimization of a VFDR missile is formulated considering radar FOV constraints. The system dynamics are first presented, followed by the objective function and associated constraints. These components are then combined to define the complete problem.

2.1. System Dynamics

The missile dynamics are modeled on the longitudinal plane as shown in Eqs. 1–5. Although an actual missile operates in three-dimensional space, trajectory optimization is performed in a two-dimensional setting because longitudinal maneuver mainly affects flight performance, owing to air density variations with altitude.

$$\dot{x} = V \cos \gamma \tag{1}$$

$$\dot{h} = V \sin \gamma \tag{2}$$

$$\dot{V} = \frac{-D + T\cos\alpha}{m} - g\sin\gamma \tag{3}$$

$$\dot{\gamma} = \frac{L + T \sin \alpha}{mV} - \frac{g \cos \gamma}{V} \tag{4}$$

$$\dot{m} = -\dot{m}_f \tag{5}$$

Where

$$L = \left(\frac{1}{2}\rho V^2 S_{ref}\right) \left(C_{L_{\alpha}}\alpha\right) \tag{6}$$

$$D = \left(\frac{1}{2}\rho V^2 S_{ref}\right) \left(C_{D_0} + K(C_{L_\alpha}\alpha)^2\right) \tag{7}$$

$$T = T(M, h, \alpha, AF) \tag{8}$$

$$\dot{m}_f = \frac{\dot{m}_a}{AF} = \frac{\rho(h)VI(\alpha)}{AF} \tag{9}$$

With Eqs. 1–5, the nonlinear equations of motion can be expressed as $\dot{z} = f(x,u)$ where $z = [x,h,V,\gamma,m]^T$, $u = [\alpha,AF]^T$. Here, x,h,V,γ and m denote downrange, altitude, velocity, flight path angle and mass. L and D represents lift and drag forces given in Eq. 6 and Eq. 7. T represents thrust,

HiSST-2025-0243

Mid-Course Trajectory Optimization for Variable Flow Ducted Rocket Missile under Radar Detection Angle Constraint

Copyright © 2025 by author(s)

and it depends on Mach number(M), altitude(h), angle of attack(α) and Air-to-Fuel ratio(AF). Since T is not available to drive a closed-form functional expression, it is instead provided as a tabulated dataset, based on the results reported in [8]. The gravitational constant is denoted by g. The fuel mass flow rate is represented by m_f . In this study, air mass flow rate (m_a) is modeled as a function of density, velocity and angle of attack as in Eq. 9. International Standard Atmosphere (ISA) model is employed to calculate air density and temperature, with the resulting density denoted by $\rho(h)$. The function $I(\alpha)$ is approximated as a fourth-order polynomial in the angle of attack.

2.2. Objective, Boundary conditions and Constraints

Maximizing terminal velocity or minimizing intercept time are widely recognized as effective performance metrics in the mid-course guidance phase. The former enhances the maneuverability during the terminal phase, while the latter reduces unnecessary fuel consumption caused by changes in target information. In this study, the impact of radar FOV constraints is investigated for both performance metrics—flight time minimization and terminal velocity maximization. The mathematical formulations for each objective are presented in Eq. 10 and Eq. 11.

minimize
$$J = -V(t_f)$$
 (10)

minimize
$$J = t_f$$
 (11)

The boundary conditions include the initial state of the missile, which is determined at launch time. In this study, these initial conditions are fixed as shown in Eq. 12.

$$x(t_0) = x_0, h(t_0) = h_0, V(t_0) = V_0, \gamma(t_0) = \gamma_0, m(t_0) = m_0$$
(12)

The terminal conditions must ensure that the missile reaches the PIP and satisfies the fuel constraint, as shown in Eq. 13.

$$x(t_f) = x_f, h(t_f) = h_f, m(t_f) \ge m_b$$
(13)

The path constraints for stable propulsion are defined in Eqs.14–17.

$$V_{min} \le V \le V_{max} \tag{14}$$

$$\alpha_{min} \le \alpha \le \alpha_{max}$$
 (15)

$$AF_{min} \le AF \le AF_{max} \tag{16}$$

$$\dot{m_f}_{min} \le \dot{m_f} \le \dot{m_f}_{max} \tag{17}$$

The radar FOV path constraints, illustrated in Fig. 2, are expressed as linear inequalities in Eqs. 18–19, under the following assumption: the boresight of the AESA radar is directed toward the PIP, and the positions of the fighter aircraft and the PIP are fixed. Here, l_u and l_d denote the upper and lower bounds of the radar FOV determined as shown in Fig. 2. These bounds are defined in terms of the radar look angle (θ) .

$$\frac{\partial l_u}{\partial x} \left(x - x(t_0) \right) + \frac{\partial l_u}{\partial h} \left(h - h(t_0) \right) \le 0 \tag{18}$$

$$-\frac{\partial l_d}{\partial x}(x - x(t_0)) - \frac{\partial l_d}{\partial h}(h - h(t_0)) \le 0$$
(19)

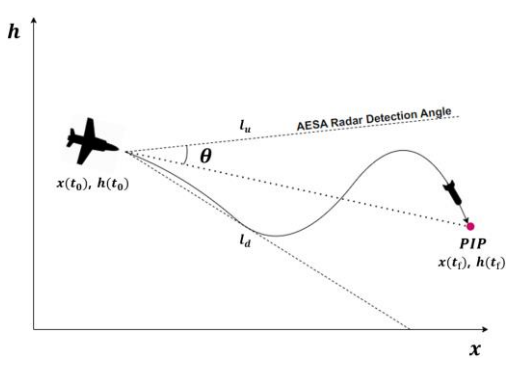


Fig 2. Radar Field of View Constraint

HiSST-2025-0243

Page | 4

Heun-Jae Lee, Boseok Kim, Chang-Hun Lee, Min-Jea Tahk, Chul Lee, Byung-Gi Kwon, Koang-Kyu Jeon

2.3. Optimal Control Problem

Using the previously defined objective function and constraints, the mid-course trajectory optimization problem is formulated as the optimal control problem given in Eq. 20.

minimize
$$-V(t_f)$$
 or t_f (20) subject to Eqs. 1–5 and Eqs. 12–19

3. Pseudo-spectral Sequential Convex Programming

In this section, the solution procedure for the aforementioned optimal control problem (Eq. 20) is presented. First, the continuous optimal control problem is discretized to a finite-dimensional optimization problem. Next, a sequential convex programming approach is employed to solve the problem. Finally, the Improved Trust Region Method, with some modifications, is incorporated to enhance the convergence properties.

3.1. Pseudo-spectral discretization

In this study, the Legendre-Gauss-Radau (LGR) pseudospectral method is employed for discretization due to its numerical stability [9]. The N nodes $[\tau_1, ..., \tau_N]$ are obtained as the roots of Eq. 22, derived from Nth-order Legendre polynomial in Eq. 21. These nodes are distributed over the interval [-1,1)

$$P_N(x) = \frac{1}{2^N N!} \frac{d^N}{dx^N} (x^2 - 1)^N$$
 (21)

$$P_{N-1}(\tau) + P_N(\tau) = 0 (22)$$

The time domain is normalized to interval [-1,1] using the affine transformation of $t=\frac{t_f-t_0}{2}\tau+\frac{t_f+t_0}{2}$. By incorporating additional (N+1)th node $\tau_{N+1}=1$, (N+1) nodes $[\tau_1,\dots,\tau_{N+1}]$ are mapped to the normalized time domain [-1,1]. States, control inputs, objectives, boundary conditions and path constraints are discretized by enforcing them at each node, as shown in Eqs. 23–29. Here, $Z=[x,h,V,\gamma,m]^T$, $U=[\alpha,AF]^T$, $\eta=t_f-t_0$. The subscript $n=1,\dots N+1$ denotes node index, which corresponds to $[\tau_1,\dots,\tau_{N+1}]$.

States and control inputs

$$[Z_1, \dots, Z_{N+1}]^T, [U_1, \dots, U_N]^T$$
 (23)

Objectives

minimize
$$J = -V(\tau_{N+1})$$
 or $J = \eta$ (24)

Boundary conditions

$$Z_1 = [x_0, h_0, V_0, \gamma_0, m_0]^T, \ Z_{N+1} = [x_f, h_f, \sim, \sim, \sim]^T$$
(25)

Path Constraints

$$V_{min} \le V_n \le V_{max} \tag{26}$$

$$\alpha_{min} \le \alpha_n \le \alpha_{max} \tag{27}$$

$$AF_{min} \le AF_n \le AF_{max} \tag{28}$$

$$\dot{m}_{f_{min}} \le \dot{m}_{f_n} \le \dot{m}_{f_{max}} \tag{29}$$

$$\frac{\partial l_u}{\partial x}(x_n - x_0) + \frac{\partial l_u}{\partial h}(h_n - h_0) \le 0$$
(30)

$$-\frac{\partial l_d}{\partial x}(x_n - x_0) - \frac{\partial l_d}{\partial h}(h_n - h_0) \le 0$$
(31)

In the pseudospectral method, because the dynamics contain derivatives, discretization requires an additional step. First, the state variables are approximated by Lagrange interpolating polynomials that pass through the chosen collocation nodes, as shown in Eq. 32. Then, by differentiating Eq. 32, the

equations of motion are approximated, as shown in Eq. 33.

$$y(t) \approx \sum_{i=1}^{N+1} \hat{y}_i \phi_i(t)$$
 (32)

$$\dot{y}(t) \approx \sum_{i=1}^{N+1} \hat{y}_i \dot{\phi}_i(t) \tag{33}$$

Here, y denotes an arbitrary state variable, and \hat{y}_j represents the coefficients of $\phi_j(t)$, which is equal to $y(\tau_j)$. $\phi_j(t)$ is the Lagrange interpolation polynomial that passes through $[\tau_1, ..., \tau_{N+1}]$. Enforcing the dynamics at each collocation node yields the discretized representation as shown in Eq. 34.

$$[\dot{y}(\tau_1), \dots, \dot{y}(\tau_N)]^T = D \cdot Y = \frac{\eta}{2} F_y(Z, U) \quad \text{where} \quad D = \begin{pmatrix} \dot{\phi}_1(\tau_1) & \cdots & \dot{\phi}_{N+1}(\tau_1) \\ \vdots & \ddots & \vdots \\ \dot{\phi}_1(\tau_N) & \cdots & \dot{\phi}_{N+1}(\tau_N) \end{pmatrix}$$
(34)

Here, y denotes each state variable—namely, x, h, V, γ and m. $Y = [y_1, ..., y_{N+1}]^T$ the set of state variables. Similarly, $F_y(Z, U) = [f_y(Z(\tau_1), U(\tau_1)), ..., f_y(Z(\tau_N), U(\tau_N))]^T$ represents the system dynamics to be imposed at each node.

Now, the resulting optimization problem can be summarized as follows.

minimize
$$J=-V(\tau_{N+1})$$
 or $J=\eta$ subject to Eqs. 25–31 and Eq. 34. (35)

3.2. Linearization and Trust Region Constraints

In sequential convex programming, the original nonconvex problem is solved by iteratively convexifying the original problem and solving resulting convex subproblems. In this study, successive linearization is employed to convexify the original nonconvex problem. In the discretized optimization problem defined in Eq. 35, the dynamics and the inequality constraint on fuel mass flow rate exhibit non-convexity. Their linearized forms at (k+1)th iteration, based on the solution obtained in the previous kth iteration, are given in Eqs. 36–38, where $\frac{\partial F_i}{\partial Z}$, $\frac{\partial F_i}{\partial U}$ & $\frac{\partial m_a}{\partial Z}$, $\frac{\partial m_a}{\partial U}$ denote the Jacobian matrices of the dynamics and the air mass flow rate. Subscript n denotes nth node.

$$(D \cdot Y)_n \approx \frac{\eta}{2} F_i(Z_n^k, U_n^k) + \frac{\eta^k}{2} \frac{\partial F_i}{\partial Z} (Z_n^k, U_n^k) (Z_n^{k+1} - Z_n^k) + \frac{\eta^k}{2} \frac{\partial F_i}{\partial U} (Z_n^k, U_n^k) (U_n^{k+1} - U_n^k)$$
(36)

$$-\dot{m}_{f_{max}} \cdot AF_n^{k+1} + \dot{m}_a(Z_n^k, U_n^k) + \frac{\partial \dot{m}_a}{\partial Z}(Z_n^k, U_n^k)(Z_n^{k+1} - Z_n^k) + \frac{\partial \dot{m}_a}{\partial U}(Z_n^k, U_n^k)(U_n^{k+1} - U_n^k) \le 0$$
(37)

$$\dot{m}_{f_{min}} \cdot AF_n^{k+1} - \dot{m}_a(Z_n^k, U_n^k) - \frac{\partial \dot{m}_a}{\partial Z}(Z_n^k, U_n^k)(Z_n^{k+1} - Z_n^k) - \frac{\partial \dot{m}_a}{\partial U}(Z_n^k, U_n^k)(U_n^{k+1} - U_n^k) \le 0$$
(38)

Due to the linearization of nonlinear constraints, large changes in the solution between convex iterations are undesirable. To mitigate this issue, a second-order variable trust region constraint is employed. First, the variable s_j is defined to quantify the variation between successive iterations for each node, as shown in Eq. 39.

$$([(Z_j)^T, (U_j)^T] - [(Z_j^k)^T, (U_j^k)^T]) ([(Z_j)^T, (U_j)^T] - [(Z_j^k)^T, (U_j^k)^T])^T \le s_j \quad \text{where} \quad j = 1, \dots, N$$
 (39)

Then, for $s = [s_1, ..., s_N]$, $||s||_2$ is incorporated into the objective function with a weight ω to penalize large deviations between iterations, as shown in Eq. 40. The weight ω serves to adjust the size of the trust region.

$$\hat{J} = -V(\tau_{N+1}) + \omega^{(k+1)} ||s||_2 \quad \text{or} \quad \hat{J} = \eta + \omega^{(k+1)} ||s||_2 \quad \text{where} \quad s \triangleq [s_1, s_2, \dots, s_N]$$
 (40)

Using the above constructions, a convex subproblem for Eq. 35 is defined as follows.

minimize
$$\hat{J} = -V(\tau_{N+1}) + \omega^{(k+1)} ||s||_2$$
 or $\hat{J} = \eta + \omega^{(k+1)} ||s||_2$ subject to Eqs. 25–31 and Eqs. 36–39

3.3. Improved Trust Region Method

To enhance convergence, the Improved Trust Region Method [7] is employed with some modifications. The main idea of the ITRM in [7] is twofold. First, the search direction p^k is defined as follows. $p^k = Z^{k+1} - \hat{Z}^k$. Here, Z^{k+1} denotes the solution of the (k+1)th SCP iteration and \hat{Z}^k denotes solution of the kth iteration, that is updated after kth SCP iteration. Second, a backtracking line search selects a step size to update solution from the SCP iteration. The purpose of the backtracking line search at this stage is to sufficiently decrease the merit function along the search direction p^k . The merit function is defined as follows.

$$\phi(X^k; \mu) = J^k + \mu_1 \sum_{n=1}^N \|h(X_n^k)\|_1 + \mu_2 \sum_{n=1}^N \|\max\{g(X_n^k), 0\}\|_1$$
(42)

 $X^k = \{Z^k, U^k, \eta^k\}$ is the solution of the kth iteration. The 1-norm terms represent the magnitudes of the violations of the original nonconvex equality and inequality constraints. $h(Z_n^k)$ represents the violation of the original dynamics (Eq. 34), in the kth iteration. Similarly, $\max\{g(Z_n^k), 0\}$ denotes the violation of the original inequality constraints (Eq. 29), in the kth iteration. μ_1 and μ_2 denote weights for each term to enhance feasibility of updated solution.

In ITRM, the predicted and exact decreases of the merit function are compared after each iteration to update the trust-region weight. If the predicted decrease is close to the exact decrease—indicating that the nonlinear constraint violation due to linearization is small—the trust region is expanded; otherwise, the trust region is reduced. Meanwhile, for adjusting the trust region, the predicted and actual decreases are typically computed based on Z^{k+1} , rather than the updated solution \hat{Z}^{k+1} . On this basis, the trust-region weight is then updated through multiplication with a constant factor. While this scheme has been shown to be effective, it may not fully capture the quantity $\hat{Z}^{k+1} - Z^k$, which can also be interpreted as the practically realized trust-region size at the (k+1)th iteration. Motivated by this observation, the proposed method introduces a trust-region weight update algorithm that is based on the quantity $\hat{Z}^{k+1} - Z^k$, which is proportional to the step size of the backtracking algorithm. The procedure of the proposed method is as follows.

First, following [7], define the search direction as Eq. 43.

$$p^k = Z^{k+1} - \hat{Z}^k (43)$$

Next, a line search is performed to select a step size that ensures a sufficient decrease in the merit function. The merit function is defined as Eq. 42. For the line search algorithm, Armijo's rule is adopted. Starting from $\zeta^k = 1$, the step size is reduced until the sufficient decrease condition in Eq. 44 was satisfied.

$$\phi(Z^k + \zeta^k p^k; \mu) \le \phi(Z^k; \mu) + \lambda \zeta^k \nabla_{n^k} \phi(Z^k; \mu) \tag{44}$$

The gradient of the merit function, $\nabla_{p^k}\phi$, along the search direction p^k , is given in Eq. 45, which follows the formulation proposed in [7].

$$\nabla_{n^k} \phi(Z^k; \mu) = J^{k+1} - \phi(Z^k; \mu) - \mu_2 \sum_{n=1}^N \|\phi(g(Z_n^k)) \cdot g_L(Z_n^{k+1})\|_{\mathcal{A}}$$
(45)

Consequently, the updated solution is given by Eq. 46, which is then used in the next SCP iteration.

$$\hat{Z}^{k+1} = Z^k + \zeta^k p^k \tag{46}$$

Next, the trust-region weight is adjusted; in the proposed method, the adjustment is performed with consideration of the $\hat{Z}^{k+1} - Z^k$, thereby reflecting the effective trust-region size realized at the at the (k+1)th iteration. Because $\hat{Z}^{k+1} - Z^k$ is proportional to ζ^k , the trust region weight is adaptively updated according to Eq. 47.

$$w^{k+1} = \beta^k w^k \quad \text{where} \quad \beta^k = \frac{c}{\zeta^k} \quad (0 < c \le 1)$$
 (47)

Meanwhile, it is assumed that a large decrease of the merit function during the step-size determination process also implies a sufficient reduction of constraint violations. Accordingly, this study does not separately compute the predicted and exact decreases. Nevertheless, these measures could readily be incorporated into the algorithm when required.

HiSST-2025-0243 Page | 7 Mid-Course Trajectory Optimization for Variable Flow Ducted Rocket Missile under Radar Detection Angle Constraint

3.4. PSCP Algorithm

The overall PSCP algorithm for trajectory optimization is summarized in Fig. 3. First, the optimal control problem is discretized using the pseudospectral method to obtain a optimization problem. Since this nonlinear problem must be linearized with respect to previous solution, an initial guess is required for the first iteration. This corresponds to the initialization step in Fig. 3. Next, the resulting convex subproblem is solved. Convergence is then checked. If achieved, the algorithm terminates. Otherwise, the proposed method calculates the step size and updates the trust-region weight. The refined solution is re-linearized to form the next convex subproblem, and this process is repeated until convergence.

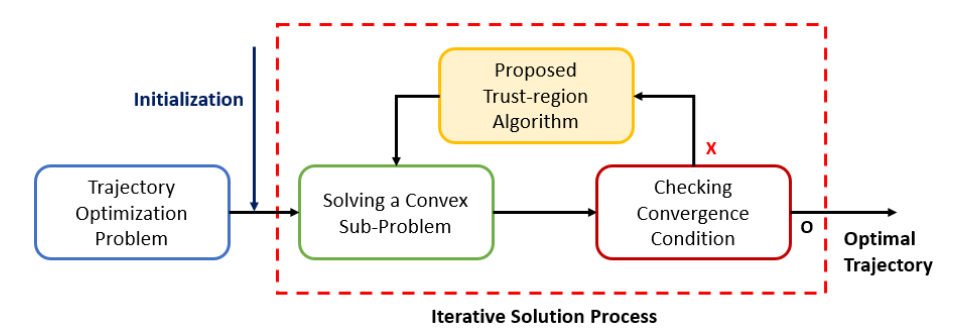


Fig 3. Entire PSCP algorithm

4. Numerical Experiments

This section examines overall characteristics of the optimal trajectory of a VFDR missile and the influence of radar FOV constraints. All test cases share identical initial conditions. Section 4.1 presents the overall characteristics of the VFDR missile's optimal trajectory without radar FOV constraints. Section 4.2 investigates the effect of radar FOV constraints with flight time minimization as a performance metric, and Section 4.3 analyzes their effect with terminal velocity maximization. Section 4.4 analyzes the performance of the proposed method.

4.1. Overall Characteristics of the VFDR missile trajectory

In this section, without imposing radar FOV constraints, the optimal trajectories are examined for three engagement conditions with a target at three different ranges: short, medium, and long. Each target altitude is assumed to be the same as those of the fighter. For each case, the trajectories are obtained with two objective functions: minimizing flight time and maximizing terminal velocity. Figs. 4 and 5 show the trajectories for flight time minimization and terminal-velocity maximization, respectively.

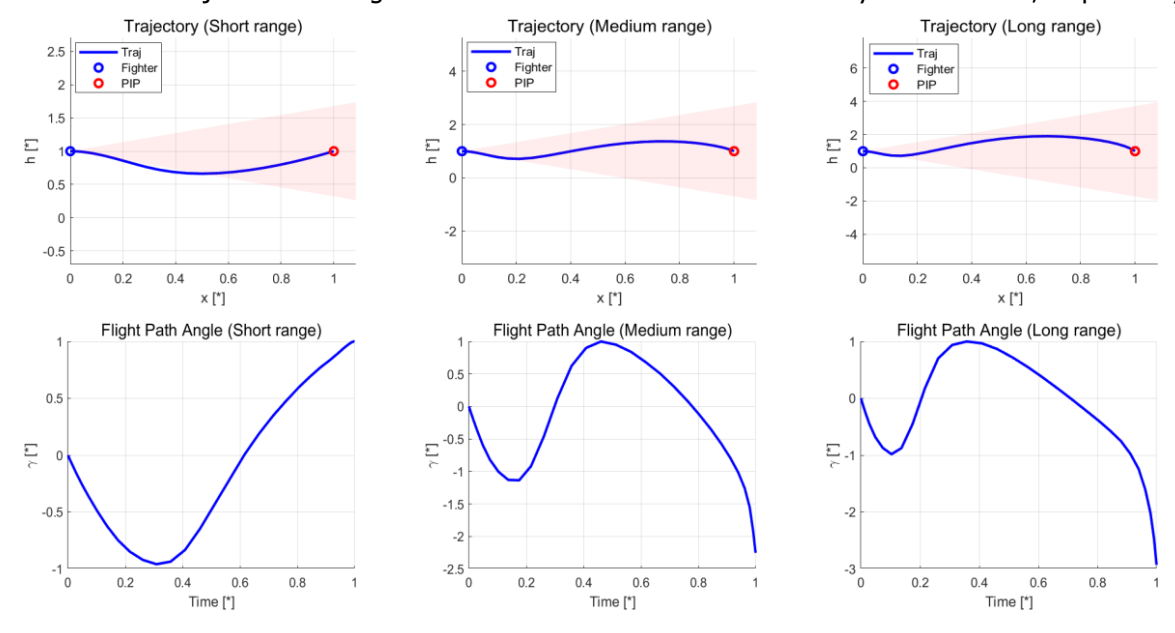


Fig 4. Trajectories without Radar FOV constraints (Flight time minimization)

HiSST-2025-0243 Page | 8 Heun-Jae Lee, Boseok Kim, Chang-Hun Lee, Min-Jea Tahk, Chul Lee, Byung-Gi Kwon, Koang-Kyu Jeon Copyright © 2025 by author(s)

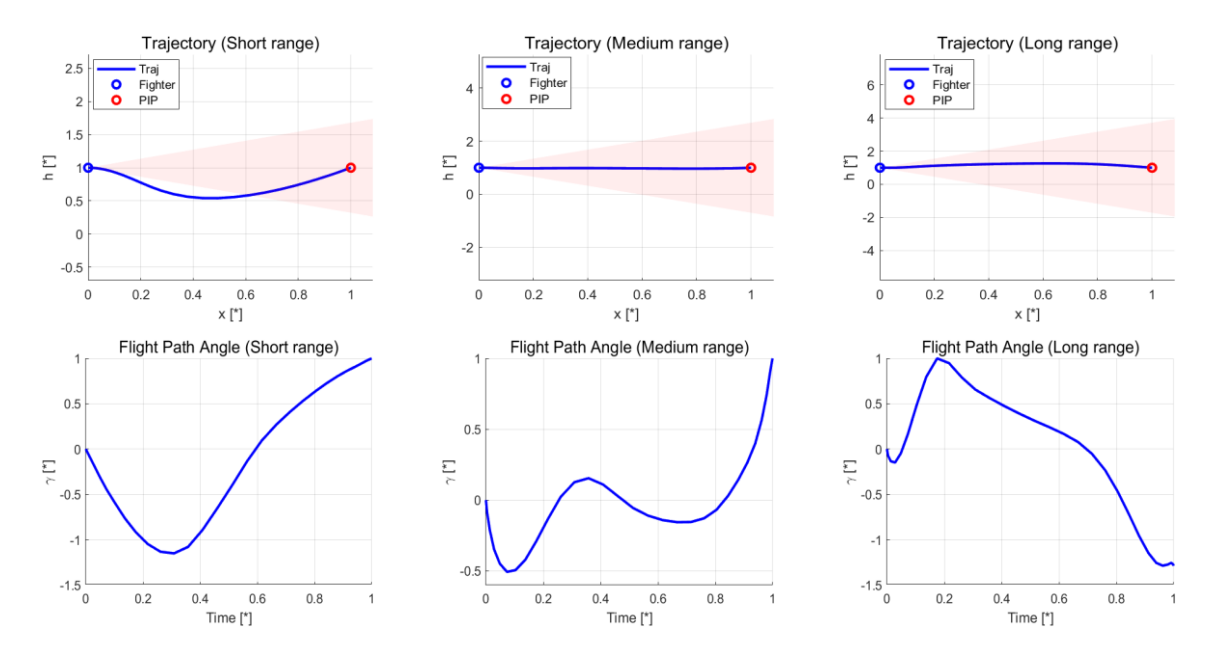


Fig 5. Trajectories without Radar FOV constraints (Terminal velocity maximization)

The optimization results indicate that the optimal trajectory of a VFDR missile has a negative flight-path angle at the start of flight, for both objectives and under all three engagement scenarios. This tendency appears to arise from the air-breathing feature. Since air is used as an oxidizer, flying through lower altitudes might be advantageous, because it increases air intake for initial acceleration. However, it should be noted that such maneuvers may cause the missile to exit the radar FOV. Of course, not all descents were steep enough to cause the missile to exit the radar FOV; in medium- and long-range engagements under terminal velocity maximization, the descent was less pronounced.

4.2. Influence of Radar FOV constraints in Flight Time Minimization

To examine the effect of radar FOV constraints for various locations of PIP, nine engagement scenarios were considered, combining three altitude levels (low, medium, and high) with three slant ranges (short, medium, and long). Optimal trajectories were computed for each engagement condition, and Table 1 summarizes whether the radar FOV constraint had an effect on optimal trajectories.

Altitude Range	Short	Medium	Long
Low	Χ	Χ	Χ
Medium	0	0	Х
High	0	0	X

Table 1. Effect of Radar FOV Constraints —flight time minimization

Four engagement conditions are affected by the radar FOV constraint, and the corresponding optimal trajectories are depicted in Figs. 6 and 7.

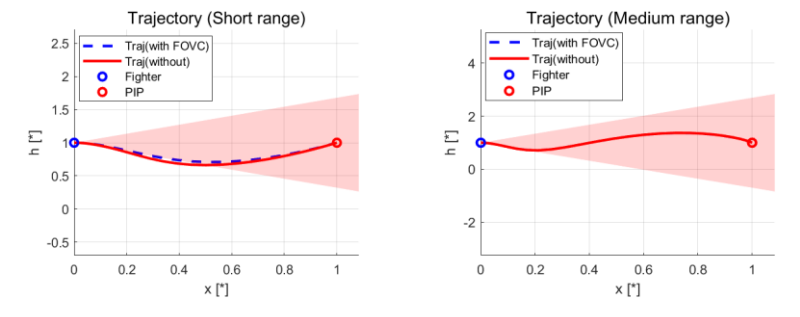
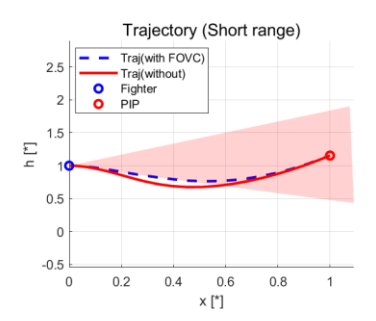


Fig 6. Trajectories toward Medium altitude targets

HiSST-2025-0243 Page | 9 Mid-Course Trajectory Optimization for Variable Flow Ducted Rocket Missile under Radar Detection Angle Constraint Copyright © 2025 by author(s)



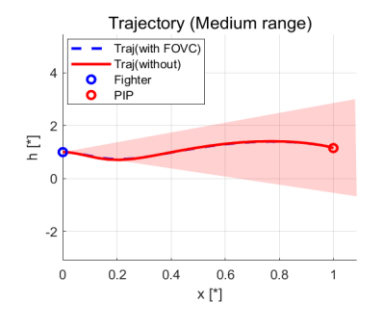


Fig 7. Trajectories toward high altitude targets

The optimization results indicate that, for both medium and high altitude targets, trajectories for short-range engagements tend to deviate more from the radar FOV limit, than medium-range engagement. This effect is most pronounced for high altitude, short-range targets, followed by medium-altitude, short-range targets. The results indicate that short-range engagements are most affected by the radar FOV constraint, and this effect is increased in higher target altitudes.

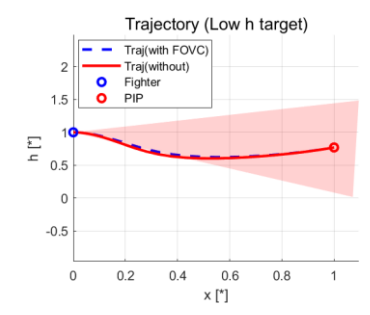
4.3. Influence of Radar FOV constraints in Terminal Velocity Maximization

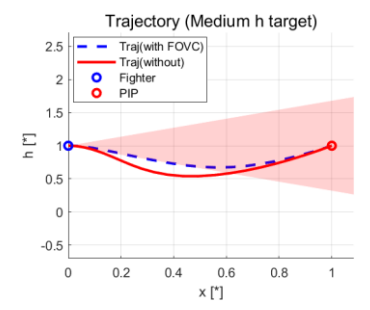
To assess the effect of radar FOV constraints under the terminal velocity maximization objective, nine engagement scenarios—identical to those in Section 4.2—were considered. Optimal trajectories were computed for each engagement condition, and Table 2 summarizes whether the radar FOV constraint had an effect on optimal trajectories.

Table 2. Effect of Radar FOV Constraints — terminal velocity maximization

Altitude Range	Short	Medium	Long
Low	0	Χ	Χ
Medium	0	Χ	Χ
High	0	Х	Х

Three engagement conditions are affected by the radar FOV constraint, and the corresponding optimal trajectories are depicted in Fig. 8





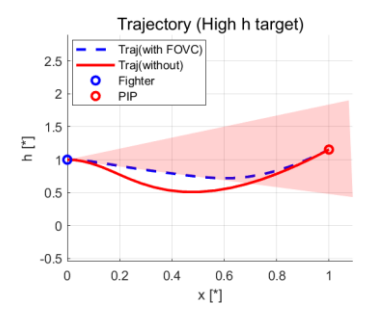


Fig 8. Trajectories toward short-range targets

The optimization results indicate that, when maximizing terminal velocity, initial descent maneuvers for short-range targets are more pronounced than in the flight time minimization case. This appears particularly evident in the optimization results for low altitude targets. However, for medium and long-range targets, the radar FOV constraint has no effect on the optimal trajectory under the terminal-velocity-maximization objective, as anticipated from the results in Section 4.1.

4.4. Performance Analysis of the Proposed Algorithm

In this section, the performance of the proposed modification for ITRM is analyzed. For performance evaluation, the same optimization procedure was carried out using the ITRM proposed in [7], and the results were compared. The analysis was conducted over the nine engagement scenarios introduced in Section 4.2. The number of SCP iterations under the trust region method was compared, and the

decreasing trends of the objective and merit functions were illustrated. The resulting optimal trajectories were presented also. In most cases, the optimal trajectories were found to be nearly identical; as a representative case, the short range, medium-altitude scenario, under the objective of velocity maximization is represented.

The analysis results for the number of SCP iterations of each algorithm are presented in Table 3. In the velocity maximization problem, the proposed method reduced the average number of iterations by 55.9%, compared to ITRM. For the flight time minimization problem, the average reduction was 63.1%. The improvement in performance may be attributed to the use of a more adaptive algorithm that, as explained earlier, adjusts the trust region weight by taking into account the finally updated solution.

Objective Algorithm	ITRM	Proposed
Velocity maximization	21.1	9.3
Flight time minimization	45.8	19.6

Table 3. Comparison of Average Iteration Counts Across Algorithms

To evaluate the validity of the proposed algorithm, an analysis was conducted for a representative case: velocity maximization for short range and medium altitude target. As shown in Fig. 9, the merit function converged to the objective function, indicating that the optimization proceeded while satisfying the constraints. In the right panel of Fig. 9, the magnitude of the trust region constraints exhibited a decreasing trend, which suggests that the algorithm converged in a stable manner. Fig. 10 indicates that nearly identical optimal trajectories were obtained for both algorithms.

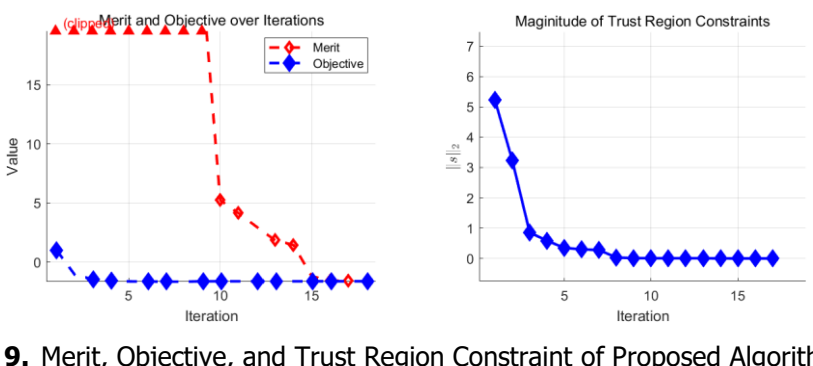


Fig 9. Merit, Objective, and Trust Region Constraint of Proposed Algorithm

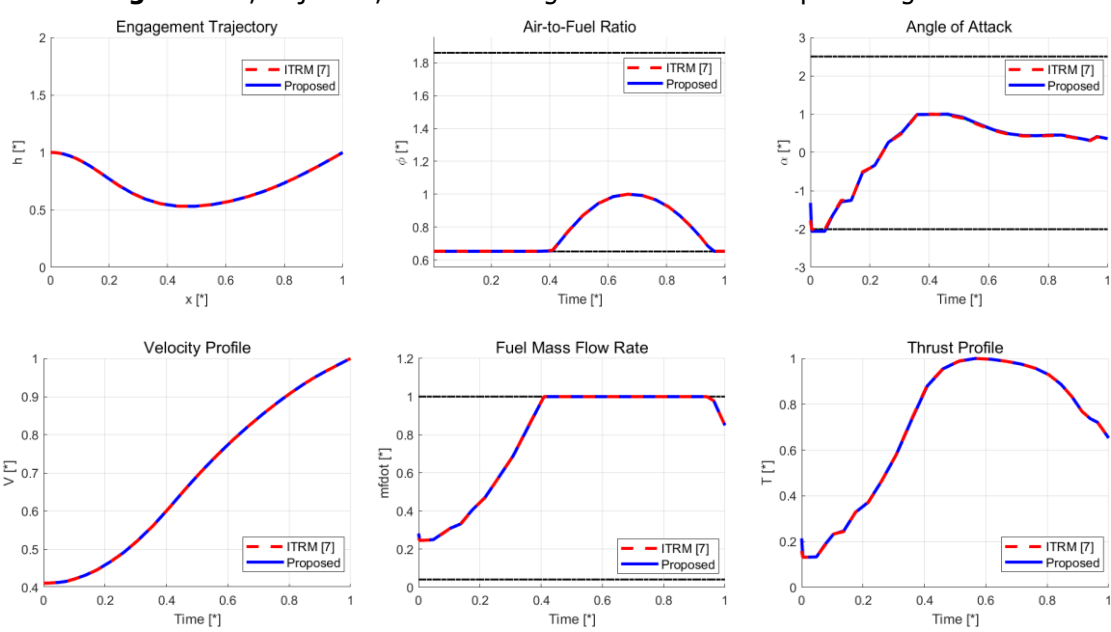


Fig 10. Comparison of Optimized Trajectories and Profiles: ITRM [7] and Proposed

Variations of the merit function and the objective function over iterations were compared for two methods: ITRM [7] and the proposed method. Figure 11 shows the merit function values over iterations, where the proposed method exhibited a more rapid decrease. In addition, the objective function converged to similar values in both cases. Figure 12 illustrates the objective function over iterations, indicating that the proposed algorithm converged faster while yielding almost identical final objective values.

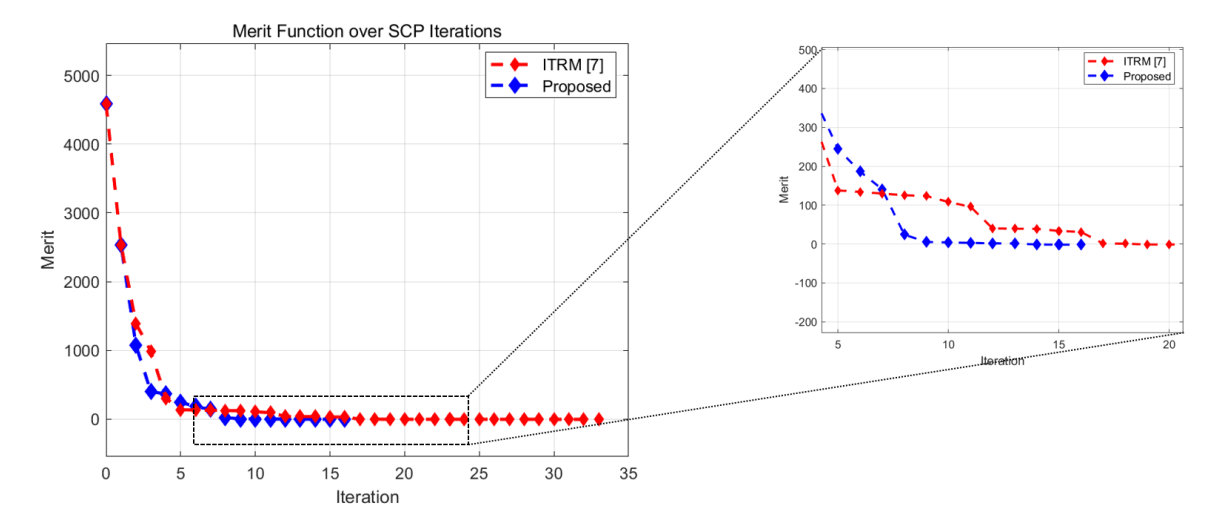


Fig 11. Merit Function value of each Algorithm

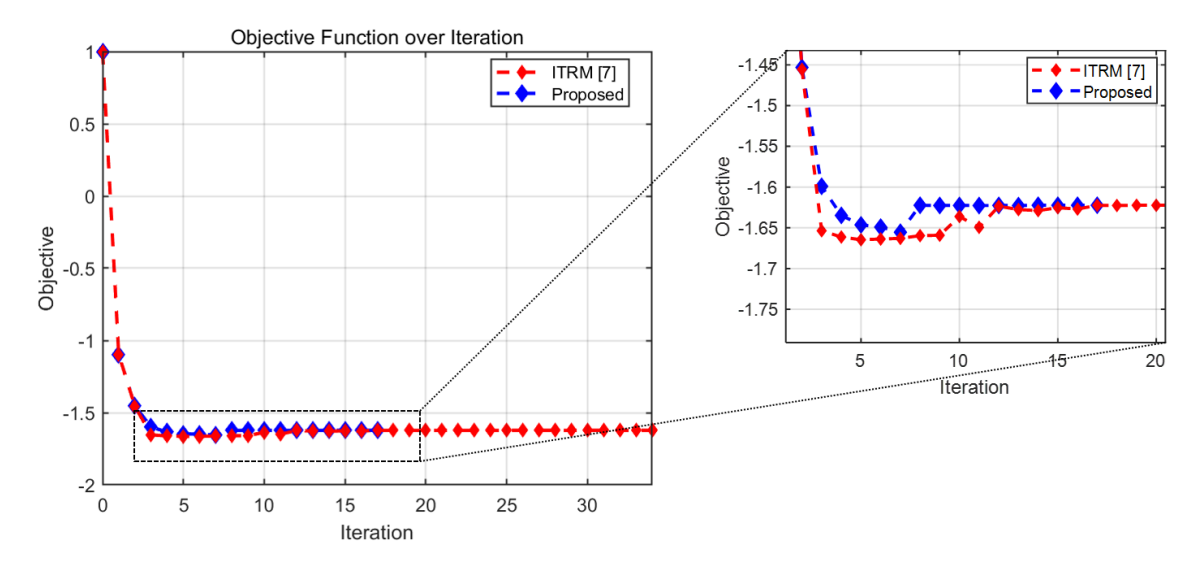


Fig 12. Objective Function value of each Algorithm

5. Conclusions

Based on the trajectory optimization using the PSCP algorithm, this paper analyzed the effect of the radar FOV constraint for various PIP locations under two different objective functions. The results indicate that, for both terminal velocity maximization and flight time minimization, short-range engagements tend to produce an initial descent in the optimal trajectory, which may cause the missile to exit the radar FOV. This tendency is more pronounced in the terminal velocity maximization case. In addition, the results indicate that higher target altitudes lead to a greater descent at the beginning of flight, for both objectives. These findings suggest that, for certain PIP locations—especially short-range engagements—the radar FOV constraints must be considered to maintain the data link between the fighter and the missile. In addition, to further enhance convergence, some modifications for existing ITRM [7] is proposed. Numerical experiments show that, for the given problem, the proposed algorithm

HiSST-2025-0243 Page | 12 Heun-Jae Lee, Boseok Kim, Chang-Hun Lee, Min-Jea Tahk, Chul Lee, Byung-Gi Kwon, Koang-Kyu Jeon

reduces the number of iterations required for convergence by about 50% compared with existing method.

Future work will focus on 3D simulations to validate the presented trajectories, incorporating both fighter and target maneuvers into the optimization process. The ultimate goal is to develop a closed-loop simulation framework using the proposed guidance techniques.

Acknowledgements

This work was partly supported by the research project titled "Study on the Operational Concept of Long-Range Air-to-Air Missiles Considering AESA Radar Integration Capability" funded by LIG Nex1, and by the Korea Aerospace Research Institute (KARI)'s own research project titled "Development of Control Performance Analysis Program for Spaceplanes". We would like to express our gratitude for the support.

References

- 1. Alan, A., Yildiz, Y., Poyraz, U.: Adaptive pressure control for use in variable-thrust rocket development. arXiv (2017). https://doi.org/10.48550/arXiv.1705.01849
- 2. Calise, A.J.: Singular perturbation techniques for on-line optimal flight-path control. Journal of Guidance and Control 4(4), 398–405 (1981)
- 3. Briggs, M.M.: Near-optimal midcourse guidance for air-to-air missiles. Journal of Guidance and Control 13(A), 596–602 (1990)
- 4. Liu, X., Shen, Z., Lu, P.: Entry trajectory optimization by second-order cone programming. Journal of Guidance and Control and Dynamics. 39(2), 227–241 (2016)
- 5. Sagliano, M.: Pseudospectral convex optimization for powered descent and landing. Journal of Guidance and Control and Dynamics. 41(2), 320–334 (2018)
- 6. Wang, Z., Lu, Y.: Improved sequential convex programming algorithms for entry trajectory optimization. Journal of Spacecraft and Rockets 57(6), 1373–1386 (2020)
- 7. Kim, B., Lee, C.-H.: Optimal midcourse guidance for dual-pulse rocket using pseudospectral sequential convex programming. Journal of Guidance and Control and Dynamics. 46(7), 1425–1436 (2023)
- 8. Lee, Y.-K., Sung, H.-G., Lee, C.-H.: Performance analysis of a ducted rocket under various flight conditions. Int. J. Aeronaut. Space Sci. 26, 674–687 (2025)
- 9. Garg, D., Patterson, M.A., Hager, W.W., Rao, A.V., Benson, D.A., Huntington, G.T.: A unified framework for the numerical solution of optimal control problems using pseudospectral methods. Automatica 46(11), 1843–1851 (2010)

HiSST-2025-0243 Page | 13 Mid-Course Trajectory Optimization for Variable Flow Ducted Rocket Missile under Radar Detection Angle Constraint